in a rather convincing way that the pure antiferromagnetic antiparallel coupling between the Dy and Co sites is an oversimplification. The results indicate that probably the dysprosium magnetic moment is decreasing and changing angle relative to the cobalt magnetic moment when the temperature is raised. Such a picture is in agreement with observed spin structure in $HoCo_5$.[18,19]

The observed effective magnetic field acting on Dy nuclei in $DyNi_5$ is 95% of the free-ion value calculated from paramagnetic compounds. This corresponds to a magnetic moment of 9.3 μ_B. The reported[8] magnetic measurements up to 14 000 Oe yield a value of 7.7 μ_B per formula unit of $DyNi_5$. Because of the lack of saturation, measurements were made in fields up to 80 kOe. A value of 8.6 μ_B was thus obtained.[20] Since at 4°K we might still not be at saturation (the Néel point is 15°K), the value of 9.3 μ_B is a lower limit for the saturated dysprosium magnetic moment. If during the bulk magnetization measurements, saturation was reached, the present results show that the nickel sites in $DyNi_5$ carry a moment above 0.7 μ_B, in contrast to the assumption that the Ni is neutral in this compound, as suggested by the early bulk magnetization measurements[8] on which Bleaney's theoretical investigation[21] was based. The high magnetic moments of Dy^{3+} in $DyNi_5$ and $DyNi_2$[9] suggest that crystalline-field effects may not be important in these crystals.[22]

[18] Williams James, Remy Lemaire, and Felix Bertaut, Compt. Rend. **255**, 896 (1962).

[19] In $HoCo_5$, neutron-diffraction measurements (see Ref. 18) show that the Co moments lie along the C axis at 4.2 and 300°K, while the Ho moments are at 22° to the C axis at 4.2°K and 90° to the C axis at 300°K.

[20] H. J. Williams, E. A. Nesbitt, and R. C. Sherwood (private communication).

ACKNOWLEDGMENTS

We are grateful to G. K. Wertheim, H. H. Wickman, H. J. Williams, E. A. Nesbitt, and R. C. Sherwood for useful discussions and to D. Dorsi for the preparation of the alloys.

[21] B. Bleaney, Proc. Phys. Soc. **82**, 469 (1963).

[22] B. Bleaney, Proc. Roy. Soc. **276**, 28 (1963).

PHYSICAL REVIEW VOLUME 140, NUMBER 1A 4 OCTOBER 1965

Linear-Network Model for Magnetic Breakdown in Two Dimensions*

W. G. CHAMBERS†

Physics Department, Texas A & M University, College Station, Texas

(Received 8 February 1965; revised manuscript received 25 May 1965)

A heuristic model is set up for magnetic breakdown in a two-dimensional rectangular lattice at right angles to an applied magnetic field. The model is an adaptation of a method due to Pippard to a set of coupled ordinary differential equations derived from the Schrödinger equation. A linear-chain network is set up. This network can also be derived from Pippard's two-dimensional network and it suggests a simple way to compute the energy bands not only when the number F of flux quanta through a unit cell is the reciprocal of an even integer (the case treated by Pippard) but also when F is any rational fraction. Numerical computations of the energy bands suggest that in the latter case the electron wave moves on large orbits which might be called "hyperorbits." These hyperorbits may be open in a rectangular lattice and may give a resonant open-orbit ultrasonic attenuation. It is also found that when a free-electron Landau level is broadened by the lattice, it splits into two bands separated by a gap. This gap moves through the states from the Landau level as F is changed and may give rise to new de Haas–van Alphen periods. The physical cause of this gap is discussed.

1. INTRODUCTION

RECENTLY, Pippard[1,2] has considered the problem of magnetic breakdown[3] in terms of the Bragg reflection of an electron moving in circular orbits in a magnetic field. An electron may be flipped from one orbit to another and its motion is confined to a periodic network of coupled orbits. Phase memory is not lost in these reflections and the phase coherence must be taken into account. In between the points where Bragg reflection can take place the effect of the lattice is ignored and the wave functions are taken to be those of a free electron in a magnetic field. The strength of the reflections is a parameter in the calculation. If this parameter is zero the model represents a situation of total breakdown. If it is unity the model represents approximately the quasiclassical situation without breakdown.

Pippard's models describe the motion of an electron in a two-dimensional "metal" with a uniform magnetic field perpendicular to its plane. The states are labelled

* Work supported by The Robert A. Welch Foundation, Houston, Texas.

† Present address: Physics Department, University of Texas, Austin, Texas.

[1] A. B. Pippard, Proc. Roy. Soc. (London) **A270**, 1 (1962).

[2] A. B. Pippard, Phil. Trans. Roy. Soc. London **A256**, 317 (1964). Unless indicated otherwise, all references to Pippard's work will be to this article.

[3] M. H. Cohen and L. Falicov, Phys. Rev. Letters **7**, 231 (1961).

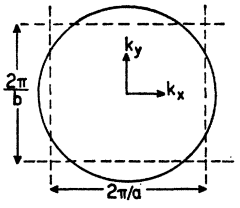

FIG. 1. Bragg reflection "planes" in relation to free-electron Fermi "surface."

by a "magnetic wave vector" similar to a Bloch wave vector. When the periodic potential is a function of both coordinates such a wave vector can be defined only if the magnetic field is such that the number F of flux quanta through a unit cell is a rational fraction. However, Pippard only considered the cases where F is the reciprocal of an even integer. It is the purpose of this paper to investigate what happens in between, for other rational values of F.

The model used in this paper is not Pippard's hexagonal model but a simpler rectangular model, and it is treated in a different way. Pippard develops a system of linear algebraic equations for the wave-function amplitudes on a two-dimensional network of coupled orbits. In this paper we set up a linear network using a system of coupled ordinary differential equations derived from the Schrödinger equation. The arguments for setting up this network are very similar to Pippard's and indeed it seems that both networks are essentially equivalent. The advantage of the linear network is that it naturally suggests a mathematical treatment of the problem which leads to straightforward computations not only when F is the reciprocal of an even integer but when it is any rational fraction. Several computations were carried out for such cases and the results indicate some new features in the energy-band structure. These are discussed in Sec. 4.

This discussion is speculative to some extent because the basic model is too simple. Thus, the author has not been able to evaluate the effects of a finite electronic relaxation time or the effects of imperfect alignment of the magnetic field.

The paper is divided as follows. Section 2 contains a derivation of the system of coupled differential equations. Section 3 describes the construction of the network and the associated algebra. Section 4 describes the results of some numerical calculations, and qualitative interpretations of these results are suggested. Section 5 is a brief summary.

2. THE MODEL AND THE BASIC EQUATIONS

The rectangular model which will be used has already been described,[4] and only the more important features will be recapitulated.

The model consists of an electron moving in a two-dimensional "metal" in the Oxy plane with a rectangular periodic potential of periods $\mathbf{a}=(a,0,0)$ and $\mathbf{b}=(0,b,0)$. A uniform magnetic field $\mathcal{H}$ is applied parallel to Oz. The vector potential will be chosen as $(-\mathcal{H}y,0,0)$ and the units will be chosen so that $2m=\hbar=1$. Then the Hamiltonian is

$$H=(p_x+hy)^2+p_y^2+V(x,y), \tag{1}$$

where $\mathbf{p}=-i\nabla$, $h=e\mathcal{H}/\hbar c$, and $V(x,y)$ is the periodic potential satisfying

$$V(x+a,y)=V(x,y+b)=V(x,y). \tag{2}$$

The "magnetic translation operators"[5] are in this gauge

$$\tau(\mathbf{a})=e^{ip_xa}=T(\mathbf{a}), \tag{3a}$$

$$\tau(\mathbf{b})=e^{i(p_y+hx)b}=T(\mathbf{b})e^{ihbx}, \tag{3b}$$

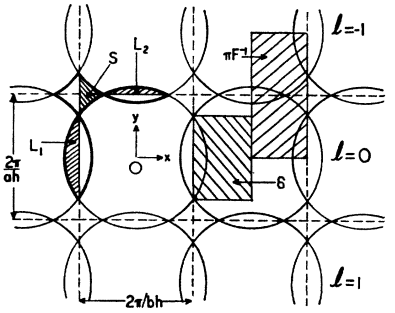

FIG. 2. System of coupled orbits in real space and certain areas expressed as multiples of the area $1/h$.

where $T(\mathbf{a})$ and $T(\mathbf{b})$ are the ordinary lattice-translation operators e^{ip_xa} and e^{ip_yb}, respectively. $\tau(\mathbf{a})$ and $\tau(\mathbf{b})$ commute with H but not with each other.

The flux per unit cell measured in flux quanta is given by

$$F=abh/2\pi. \tag{4}$$

If F is a rational fraction λ/N of two integers λ and N with no common factors, it can be shown that $\tau(\mathbf{a})$ commutes with $\tau(N\mathbf{b})\equiv\{\tau(\mathbf{b})\}^N$. Then it is possible to define a simultaneous eigenfunction and two wave numbers q_x and q_y by

$$H\Psi(\mathbf{q},\mathbf{r})=E(\mathbf{q})\Psi(\mathbf{q},\mathbf{r}), \tag{5a}$$

$$\tau(\mathbf{a})\Psi(\mathbf{q},\mathbf{r})=e^{iq_xa}\Psi(\mathbf{q},\mathbf{r}), \tag{5b}$$

$$\tau(N\mathbf{b})\Psi(\mathbf{q},\mathbf{r})=e^{iq_yNb}\Psi(\mathbf{q},\mathbf{r}). \tag{5c}$$

It can be shown that each state is N-fold degenerate, and that it is sufficient to limit $\mathbf{q}$ to a magnetic zone of dimensions $(2\pi/Na)\times(2\pi/Nb)$. The wave number q_x is treated differently from q_y. An analogy is the choice of a special axis in the theory of angular momentum.

The Fermi surface will be chosen as in Fig. 1 in relation to the Brillouin zone; the Brillouin zone is rectangular and the free-electron Fermi surface intersects each side inside the rectangle. Figure 2 shows Pippard's network construction (in real space) for this model. The orbits are linked by Bragg reflection, and when this reflection is nearly complete the orbits consist

[4] W. G. Chambers, Proc. Phys. Soc. (London) **84**, 941 (1964).

[5] E. Brown, Phys. Rev. **133**, A1038 (1964).

of two lenses $2L_1$, $2L_2$, and a hole orbit $2S$ in each unit cell.

The Bragg reflections are adequately represented by a potential

$$V(x,y)=2V_0\cos(2\pi y/b)+2V_1\cos(2\pi x/a). \quad (6)$$

The Schrödinger Eq. (5a) can be treated as follows.[6,7] Since $\tau(\mathbf{a})$ is an ordinary translation operator, $\Psi(\mathbf{q},\mathbf{r})$ depends on x in the usual manner of a Bloch function and may therefore be expanded in a Fourier series:

$$\Psi=\sum_l e^{i(lg+q_x)x}u_l(y), \quad (7)$$

where $g=2\pi/a$. Then the substitution of (7) and (6) into the Schrödinger Eq. (5a) rapidly gives a set of coupled ordinary differential equations,

$$[-d^2/dy^2+(lg+q_x+hy)^2-E]u_l +[2V_0\cos(2\pi y/b)]u_l+V_1(u_{l-1}+u_{l+1})=0. \quad (8)$$

When F [Eq. (4)] is a rational fraction λ/N, Eq. (5c) imposes boundary conditions so that

$$u_l(y+Nb)=e^{iNq_yb}u_{l+\lambda}(y). \quad (9)$$

Though the wave function $\Psi(\mathbf{q},\mathbf{r})$ is completely "smeared" in the x direction, it is possible to interpret the solutions $u_l(y)$ as representing lines of orbits parallel to Ox (Fig. 2). This interpretation is strictly valid only if V_1 is small.

3. THE NETWORK

Provided that the periodic potential in (8) is sufficiently weak, it is possible to use Pippard's concept that

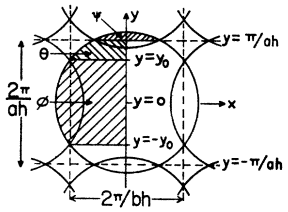

FIG. 3. Certain areas in the orbit system in real space, expressed as multiples of the area $1/h$.

the wave function is only seriously affected by the lattice in the neighborhood of those points where Bragg reflection is possible and that elsewhere the wave function is free electron-like. In this way one may use (8) to set up a one-dimensional network. It is necessary to know what phase-shifts are to be put in for the Bragg reflections and it will be assumed that the Born approximation is an adequate guide. The reason is that it is valid for very weak periodic potentials and therefore automatically deals with the effects of the choice of gauge. The free-electron wave functions will be treated by the W.K.B. (Wentzel-Kramers-Brillouin) approximation.[1] For the moment then we shall set $V_0=V_1=0$ in (8) and for convenience a new origin of the lth equation will be chosen at the center of the parabolic potential, at $y=-(q_x+lg)/h$. The classical turning points are to be ignored for the time being and we shall employ running wave functions in the W.K.B. approximation,

$$u_\pm(y)=f(y)e^{\pm iJ(y)} \quad (10)$$

with

$$f(y)=(E-h^2y^2)^{-1/4} \quad (11)$$

and

$$J(y)=\int_0^y(E-h^2\eta^2)^{1/2}d\eta. \quad (12)$$

There are two (apparently) different types of Bragg reflection, one caused by the term containing V_0, and the other by the terms containing V_1 which switch the electron from one line or orbits to the next. These reflections are considered in turn. The potential V_0 causes Bragg reflection at the points $\pm y_0$ in Fig. 3. Suppose a wave $u_+(y)$ comes up to y_0 and is scattered downwards. The scattering amplitude is given by a matrix element. It must be remembered that the origin has been shifted, so that the potential must be changed. It can be written as $2V_0\cos[2\pi(y/b)-\alpha_l]$, where

$$\alpha_l=\alpha+2\pi lN/\lambda \quad (13)$$

with

$$\alpha=2\pi q_x/bh. \quad (14)$$

The scattering amplitude is proportional to the matrix element

$$\int u_-^*(y)2V_0\cos[2\pi(y/b)-\alpha_l]u_+(y)dy.$$

The integral has stationary phase points at $\pm y_0$, but at the moment we are only interested in the point $+y_0$. The contribution to the integral from the neighborhood of this point may be obtained by the method of steepest descent. The result may be written as

$$Ke^{i[2J(y_0)+\alpha_l-\delta]}, \quad (15)$$

where

$$\delta=2\pi y_0/b, \quad (16)$$

and where K is a slowly varying function of energy with a nearly constant phase. The phase $2J(y_0)$ in (15) arises from the choice of phase for $u_\pm(y)$ and would vanish if

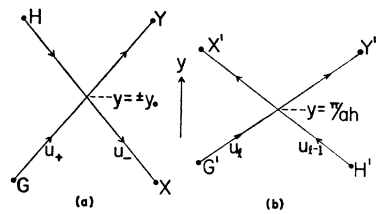

FIG. 4. Wave-function amplitudes to be related at junctions representing Bragg reflections by (a) the y component V_0 of the periodic potential, and (b) the x component V_1 of the periodic potential.

[6] P. G. Harper, Proc. Phys. Soc. (London) **A68**, 879 (1955).
[7] J. Zak, Phys. Rev. **136**, A1647 (1964).

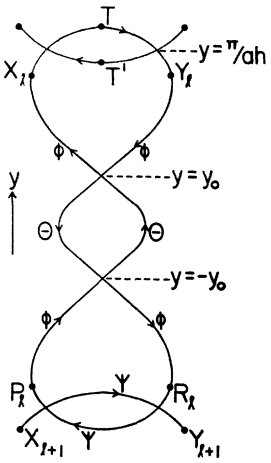

FIG. 5. The lth link of the network and wave-function amplitudes to be related. Also shown are the propagation phase shifts θ, φ, ψ, classical turning points T, T', and the connections to the $(l\pm1)$th links.

the origin of integration in (12) were put at y_0. The phases α_l and $-\delta$ should be regarded as being due to the Bragg reflection. We may ignore phase shifts which are almost independent of the parameters of the calculation, but α_l depends sensitively on the wave number q_x and on the label l of the line of orbits, and so it must be included. δ depends on the energy through the value of y_0 (Fig. 3).

The Bragg reflection is represented by a junction similar to those in Pippard's model. At the junction a wave traveling upwards with unit amplitude may be reflected with amplitude q or be transmitted with amplitude p, and similar coefficients may be defined for a wave traveling downwards. These coefficients must obey certain conservation or unitarity conditions.[1] In contradistinction to Pippard's convention the transmission p was taken as real and the reflection q as intrinsically imaginary. However q must also have an extra phase $(\alpha_l-\delta)$. Figure 4(a) shows how the junction is drawn and the amplitudes to be related. For $y=+y_0$ we shall set down the following relations which obey the conservation conditions:

$$X=(1-Q_1^2)^{1/2}H+iQ_1e^{i(\alpha_l-\delta)}G, \tag{17a}$$

$$Y=(1-Q_1^2)^{1/2}G+iQ_1e^{-i(\alpha_l-\delta)}H. \tag{17b}$$

Here Q_1 is real and lies between 0 and 1, and represents the strength of the reflection. A similar result applies to the junction at $y=-y_0$, and the only difference is that the sign of δ is changed.

The terms in (8) containing V_1 couple the equations and this coupling may also be regarded as a Bragg reflection at $y=\pm\pi/ah$. The coupling may be calculated using the Born approximation. This time no phase shifts need be introduced. The coupling is represented by a junction as in Fig. 4(b) and the amplitudes will be assumed to satisfy

$$X'=(1-Q_2^2)^{1/2}H'+iQ_2G', \tag{18a}$$

$$Y'=(1-Q_2^2)^{1/2}G'+iQ_2H', \tag{18b}$$

with Q_2 real and between 0 and 1.

Figure 5 then shows how the linear network is to be set up. The diagram represents the lth link corresponding to the lth equation in (8) and the coupling to the $(l\pm1)$th equations. The classical turning points are represented by points like T and T', but it is not necessary to bother about putting in any phase shifts here. A number λ of such links is to be joined and the boundary condition (9) is used. The propagation phase shifts θ, φ, ψ in Fig. 5 correspond to certain areas (expressed as multiples of h^{-1}) in Fig. 3 and represent W.K.B. phase integrals of the type (12). In this way the wave numbers q_x and q_y are related to the parameters of the model.

Before the algebraic problems are described it should be emphasized that this model is essentially equivalent to Pippard's model in spite of its rather different structure. If Pippard's model is set up for the rectangular lattice with the Landau gauge of Sec. 2, then the network of Fig. 5 can be derived.

The algebra for the network is straightforward. We may express the amplitudes above any given junction in terms of amplitudes below the junction by a 2×2 matrix. By multiplying such matrices together it is found that the amplitudes X_l, Y_l, P_l, and R_l in Fig. 5 are related by

$$\begin{pmatrix}P_l\\R_l\end{pmatrix}=\mathbf{K}_l\begin{pmatrix}X_l\\Y_l\end{pmatrix}, \tag{19a}$$

where $\mathbf{K}_l$ is a matrix function of α given by

$$\mathbf{K}_l(\alpha)=\begin{pmatrix}A & Be^{-i\alpha l}\\ B^*e^{i\alpha l} & A^*\end{pmatrix} \tag{19b}$$

with

$$A=(1-Q_1^2)^{-1}[e^{-i(2\theta+\varphi)}+Q_1^2e^{i(\varphi-2\theta-2\delta)}], \tag{20a}$$

$$B=-2iQ_1(1-Q_1^2)^{-1}\cos(\varphi-\delta), \tag{20b}$$

and with α_l given by (15) and (16). The matrix $\mathbf{K}_l$ has the form

$$\begin{pmatrix}Z_1 & Z_2\\ Z_2^* & Z_1^*\end{pmatrix}, \tag{21}$$

where Z_1 and Z_2 are complex numbers. The product of two such matrices also has the same form, so that products of such matrices only involve calculating two complex numbers rather than four. It is also readily shown that $\det\mathbf{K}_l=1$.

It is better to define the coefficients of $\mathbf{K}_l$ in terms of the areas of the lens orbits and of the hole orbit. We write L_1, L_2, S for *half* the areas of the lens orbits and of the hole orbit, respectively, expressed as multiples of h^{-1}. Then it is readily found (by using Figs. 2 and 3) that

$$S=\pi F^{-1}-\delta-2\theta, \tag{22a}$$

$$L_1=\varphi-\delta, \tag{22b}$$

$$L_2=\psi. \tag{22c}$$

It is also useful to define

$$\Sigma = S - \pi F^{-1}. \tag{22d}$$

Then instead of (20) we may write

$$A = (1-Q_1^2)^{-1} e^{i\Sigma}(e^{-iL_1} + Q_1^2 e^{iL_1}), \tag{23a}$$

$$B = -2iQ_1(1-Q_1^2)^{-1}\cos L_1. \tag{23b}$$

In much the same way it is possible to relate the amplitudes X_{l+1}, Y_{l+1}, P_l, R_l in Fig. 5 by

$$\begin{pmatrix} X_{l+1} \\ Y_{l+1} \end{pmatrix} = \mathbf{M} \begin{pmatrix} P_l \\ R_l \end{pmatrix}, \tag{24a}$$

where

$$\mathbf{M} = \frac{1}{b^*} \begin{pmatrix} a & -1 \\ 1 & -a^* \end{pmatrix} \tag{24b}$$

with

$$a = (1-Q_2^2)^{-1}(e^{-iL_2} + Q_2^2 e^{iL_2}), \tag{24c}$$

$$b = -2iQ_2(1-Q_2^2)^{-1}\cos L_2. \tag{24d}$$

The matrix $\mathbf{M}$ also has the form (21) and its determinant is equal to one.

We then just multiply the matrices for the propagation down the network and use the boundary condition (9) which gives

$$\begin{pmatrix} X_\lambda \\ Y_\lambda \end{pmatrix} = e^{-i\lambda\beta} \begin{pmatrix} X_0 \\ Y_0 \end{pmatrix} \tag{25}$$

where

$$\beta = 2\pi q_y / ah. \tag{26}$$

We obtain a secular equation with a 2×2 determinant

$$\det[\mathbf{I}e^{-i\lambda\beta} - \mathbf{T}(\alpha)] = 0, \tag{27}$$

where $\mathbf{I}$ is the 2×2 unit matrix and where

$$\mathbf{T}(\alpha) = \prod_l [\mathbf{M}\mathbf{K}_l(\alpha)], \tag{28}$$

where the product is taken from $l=0$ to $\lambda-1$ with the higher values of l on the left. Since $\mathbf{M}$ and $\mathbf{K}_l$ have the form (21) and have unit determinant, the product $\mathbf{T}(\alpha)$ also shares these properties and in particular its trace is real. The Eq. (27) then gives

$$\cos\lambda\beta = \tfrac{1}{2}\,\mathrm{Tr}\,\mathbf{T}(\alpha). \tag{29}$$

The dependence of the trace on α appears complicated, but in the case when the lattice is square (with $Q_1=Q_2$ and $L_1=L_2$), it is apparent that α must come in symmetrically with β. Hence (29) must give

$$\cos\lambda\alpha + \cos\lambda\beta = \tfrac{1}{2}\,\mathrm{Tr}\,\mathbf{T}(0) + 1.$$

For the more general problem there does not seem to be such a short cut. A method for explicitly obtaining the terms containing α is given in the Appendix. The general result may be written

$$\gamma_1 \cos\lambda\alpha + \gamma_2 \cos\lambda\beta = \gamma_3 \tag{30a}$$

with

$$\gamma_1 = [2(1-Q_2^2)Q_1 \cos L_1]^\lambda, \tag{30b}$$

$$\gamma_2 = [2(1-Q_1^2)Q_2 \cos L_2]^\lambda, \tag{30c}$$

$$\gamma_3 = \gamma_1 + \tfrac{1}{2}\,\mathrm{Tr}\prod_l (\mathbf{Y}\mathbf{X}_l), \tag{30d}$$

where the matrix product is taken from $l=0$ to $\lambda-1$ with the higher values of l on the left, and where the matrices are given by

$$\mathbf{X}_l = \begin{pmatrix} \chi_1 & \chi_2 \\ \chi_2^* & \chi_1^* \end{pmatrix}, \quad \mathbf{Y} = \begin{pmatrix} \eta_1 & \eta_2 \\ \eta_2^* & \eta_1^* \end{pmatrix}, \tag{30e}$$

with

$$\begin{aligned} \chi_1 &= e^{i\Sigma}(e^{-iL_1} + Q_1^2 e^{iL_1}), \\ \chi_2 &= -2iQ_1 \cos L_1 e^{-2\pi i l N/\lambda}, \\ \eta_1 &= -i(e^{-iL_2} + Q_2^2 e^{iL_2}), \\ \eta_2 &= i(1-Q_2^2). \end{aligned} \tag{30f}$$

The energy bands were found in the same way as by Pippard. The areas of the orbits are assumed to vary linearly with the energy over a narrow range of energies, so we shall set

$$\begin{aligned} S &= -(2\pi n_3 x + \varphi_3), \\ L_1 &= (2\pi n_1 x + \varphi_1), \\ L_2 &= (2\pi n_2 x + \varphi_2), \end{aligned} \tag{31}$$

where x represents the energy, and where φ_1, φ_2, and φ_3 can be used to introduce relative phases. The parameters n_1, n_2, n_3 then represent the rate of change of the areas with energy. Of course S, L_1, and L_2 depend on the field h as well, but this dependence has been left out in this paper. The condition for an allowed value of x is that the quantity

$$f(x) = \gamma_3/(|\gamma_1| + |\gamma_2|) \tag{32}$$

should lie between -1 and $+1$. The above equations can be programmed for automatic computation very easily.

The quantization conditions in the cases of total breakdown ($Q_1=Q_2=0$) and of zero breakdown ($Q_1=Q_2=1$) are very easily obtained by calculating the phases acquired in propagation as a wave goes round the appropriate orbit. For the case of total breakdown the condition is that the quantity

$$2C \equiv 2L_1 + 2L_2 - 2S + 2\pi F^{-1} \tag{33}$$

should be a multiple of 2π. Here $2C$ is the area of the circular orbits in Fig. 2, expressed as a multiple of h^{-1}. Similarly, for the case of zero breakdown the condition is that $(2L_1+\pi)$, $(2L_2+\pi)$, or $2S$ should be a multiple of 2π depending on which orbit we are considering.

4. RESULTS AND CONSIDERATIONS

Some results of numerical computations based on (30) are now given and discussed. There are a large number of parameters in this model and of course some

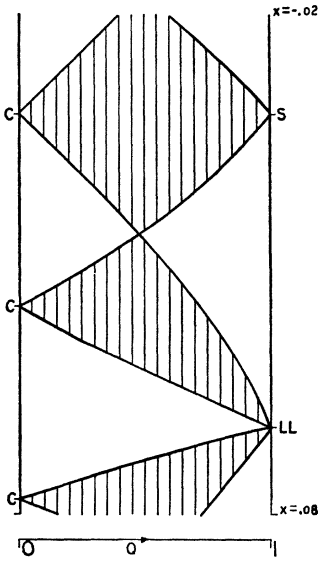

FIG. 6. Portion of energy-band structure for square lattice as a function of Q when F^{-1} is an integer. The energy variable x increases downwards. Bands are shaded.

arbitrary choice of values must be made. In order to show the energy bands in the same manner as in Pippard's paper one sets $Q_1=Q_2=Q$ and treats Q and the energy parameter x [Eq. (31)] as variables. The other parameters in (30) and (31) are kept fixed. One then shows on a graph the regions where the function f of (32), regarded as a function of x and Q, lies between -1 and $+1$. The parameters n_1, n_2, n_3 in (31) are arbitrarily chosen as

$$n_1=n_2=4, \quad n_3=5$$

throughout.

In the first computation the parameters φ_1, φ_2, φ_3 in (31) are all chosen to be zero to give a square lattice. We take a situation analogous to Pippard's, where F^{-1} is an even integer, so that $\lambda=1$ and N is even. For $Q=0$ the allowed values of x are given by $x=0$, $\pm 1/26$, $\pm 2/26$, etc. These values correspond to the free-electron Landau levels C. For $Q=1$ there are two sets of levels for $x=\pm 1/16$, $\pm 3/16$, etc., and for $x=0$, $\pm 1/10$, $\pm 2/10$, etc. The first set corresponds to the doubly degenerate lens orbits LL and the second set to the hole orbits S. Figure 6 shows how some free-electron levels C evolve into the levels LL and S as Q varies from 0 to 1. The vertical axis represents x increasing *downwards* from $x=-0.02$ to $x=+0.08$. This is a rather narrow range, but it is adequate to illustrate the general idea. The shaded areas represent the regions of the allowed values of x. It is apparent that as Q is increased the levels C broaden and then condense back into the levels S and LL. The similarity of this diagram to the diagrams shown by Pippard for the hexagonal model is evident, although the structure is simpler. The electronic velocities are given by $\mathbf{v}=\partial E/\partial \mathbf{q}$ (Ref. 2). Therefore the broad bands for $Q\approx 0.5$ signify large electronic velocities. These turn out to have the same magnitude as the Fermi velocity of the model without any applied field. Figure 7 shows the form of the energy contours in $\mathbf{q}$ space in the "magnetic Brillouin zone." They have the same structure as the energy contours in a square tight-binding model because of the form of (30a).

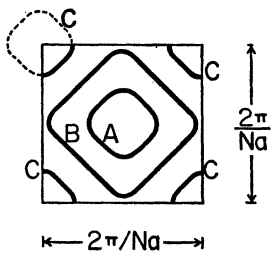

FIG. 7. Energy contours in $\mathbf{q}$ space for a square lattice when F^{-1} is an integer.

This calculation has been carried out for the case when F^{-1} is an even integer, but the band structure is unaltered if F^{-1} is an odd integer, provided nothing else is changed in (30) and (31). In general it can be shown that for this model an increase in F^{-1} by any integer does not alter the energy bands. If $F^{-1}=N/\lambda$ is increased by unity, the only difference is that γ_3 in (30) is multiplied by $(-1)^\lambda$. So it is only necessary to specify the field by two integers λ and p, where

$$p=N \text{ modulo } \lambda.$$

Figure 6 thus shows a band structure when $p/\lambda=0/1$ and F^{-1} is an integer. Figure 8 shows the case when F^{-1} has been increased by $\frac{1}{5}$, so that $p/\lambda=\frac{1}{5}$. The levels C have now been shifted relative to S and LL, because F^{-1} enters into (32). Of course, S and LL would also be shifted relative to one another if the variation of S and LL with the field h had been put into (31). For simplicity this has been ignored. As Q is increased from zero each level C breaks up into λ sub-bands,[2,4,5] five in this case. Within each set of sub-bands the central ones are comparatively broad and appear to be touching or nearly touching. Those sub-bands that are broad enough have been shaded in. It also seems that one sub-band can split off from the others and go to a different level. This point will be discussed later.

The relation between the structures in Fig. 6 and Fig. 8 is not altogether obvious, but some other computations were tried for cases like $p/\lambda=1/9$ and $1/20$, when F^{-1} is nearer an integral value than it is in Fig. 8. As in Fig. 8, each level C splits into λ sub-bands where the central ones are broad, but as the energy goes away from the central values the sub-bands are progressively narrower, and most of them are much narrower then the spacing between them. They occupy the regions of the original bands of Fig. 6 in such a way that the coarse energy density of states is not altered much. Thus it appears that the bands in Fig. 6 condense into "quasi-Landau" levels when the field is changed slightly so that F^{-1} is no longer an integer, but near an integral value. The narrowness of these sub-bands suggests that the group velocities are on the whole very low. Pippard

(private communication) has suggested a qualitative view of this phenomenon. If the magnetic field $\mathbf{h}$ has a value $\mathbf{h}_0$ so that F^{-1} is exactly an integer, then an electron wave can travel in straight lines through the structure of Fig. 2 in any direction with a speed of the same order of magnitude as the Fermi velocity. Suppose $\mathbf{h}$ is changed very slightly to a value $\mathbf{h}_1$ so that F^{-1} is very close to its original integral value. Then the residual field $\mathbf{h}_r=\mathbf{h}_1-\mathbf{h}_0$ bends the trajectories into orbits with a very large diameter. These lead to the "quasi-Landau" levels and give a very low group velocity.

One may try to go a little further and develop an approximate "semiclassical" theory for these larger orbits, which we shall call "hyperorbits." It has been shown[2] that under the effect of an electric field $\mathbf{E}$ the magnetic wave vector $\mathbf{q}$ varies as

$$d\mathbf{q}/dt=e\mathbf{E}.$$

This suggests that with a residual magnetic field $\mathbf{h}_r$ there may be an equation of motion

$$d\mathbf{q}/dt=\mathbf{v}\times\mathbf{h}_r,$$

where $\mathbf{v}=\partial E/\partial\mathbf{q}$ is the group velocity. Such a theory would be expected to work only if F^{-1} was very close to an integral value.

This theory gives at least a qualitative description of the structure of the sub-bands within a given band of the sort in Fig. 6. Figure 7 shows that for energies near the edges of a band we may have electron orbits like A or hole orbits like C in $\mathbf{q}$ space. The orbits for the central values of the energy (like B) are passing close to the zone boundaries and would be broadened by "intraband" breakdown.[8]

A computation was performed for a case when p/λ was equal to $6/31$, a value very close to $1/5$. In this case the sub-bands of Fig. 8 all broke up into six "sub-sub-bands" and another "sub-sub-band" appeared along the line of contact of the central sub-bands in each band. Most of these were much narrower than the spacing between them. This suggests that the "hyperorbits" can in turn give rise to "hyper-hyperorbits," though it is to be doubted whether this result is of great practical interest!

For general values of F^{-1} we may say that λ is "very large." Computations have been carried out for values of λ up to 40, and the sub-bands are very narrow indeed in all the cases tried. The theory suggests that the group velocities are very low because of the hyperorbits.

Let us now suppose that we have a general rectangular lattice. Then in the case when F^{-1} is an integer the energy contours in a typical band may be as shown in Fig. 9. The "semiclassical" theory discussed above suggests that if F^{-1} is changed by a small amount, open hyperorbits like B in Fig. 9 would arise and the velocities could be quite large along these hyperorbits. The direction of these orbits may vary between the x and y directions from band to band and would therefore be very sensitive to the energy.

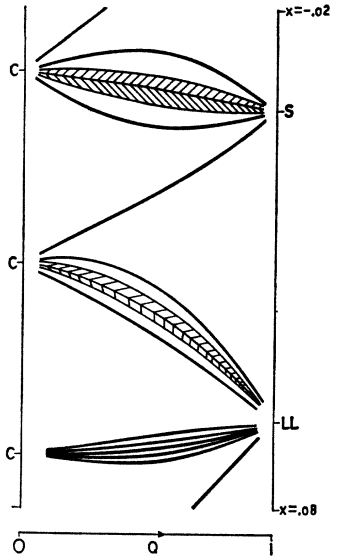

FIG. 8. Portion of energy-band structure for square lattice when F^{-1} is an integer plus $\frac{1}{2}$. Broader sub-bands are shaded. Narrower sub-bands are represented by lines.

This idea can be supported by a consideration of (30). The coefficients γ_1 and γ_2 are in general unequal, and for large values of λ their ratio is very large or very small. Hence the group velocities are almost entirely parallel either to the x axis or to the y axis. If Q_1 is equal to Q_2, but L_1 not equal to L_2, the velocities are almost entirely parallel to the x axis when $|\cos L_1|>|\cos L_2|$ and almost entirely parallel to the y axis when $|\cos L_1|<|\cos L_2|$. The direction of propagation is thus very sensitive to the energy.

A numerical computation was carried out for $p/\lambda=1/5$ with the parameters the same as for the situation shown in Fig. 8, except that the phases in (31) were chosen as $\varphi_1=0$, $\varphi_2=\pi/2$, $\varphi_3=\pi/6$. Thus L_1 is not equal to L_2 and the lattice is rectangular in effect. The phase φ_3 was altered from zero so that S would not coincide with L_2. The band structure is shown in Fig. 10, and it seems that in general the sub-bands are broader than in Fig. 8. In the neighborhood of the energy level L_1 the velocities are approximately parallel to the y axis and in the neighborhood of L_2 approximately parallel to the x axis. Several other cases were tried for rectangular lattices and the results indicated that the velocities were on the whole quite large, perhaps even of the magnitude of the Fermi velocity. These results support the concept of open hyperorbits.

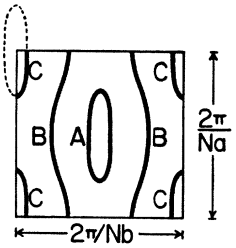

FIG. 9. Energy contours in $\mathbf{q}$ space for rectangular lattice when F^{-1} is an integer.

[8] W. G. Chambers, Proc. Phys. Soc. (London) 84, 181 (1964).

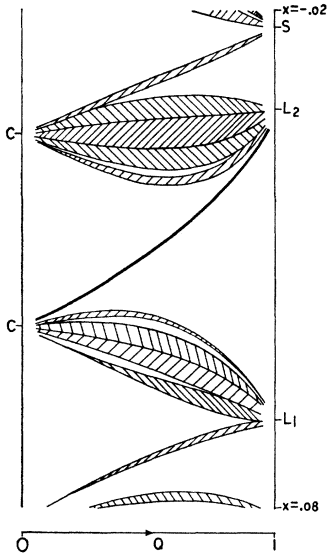

FIG. 10. Portion of energy-band structure for rectangular lattice when F^{-1} is an integer plus $\frac{1}{5}$. Broader sub-bands are shaded. Narrower sub-bands are represented by lines.

Let us now consider why in both Figs. 8 and 10 one sub-band within a given band breaks away from the others. In both of these cases we have set $p/\lambda=\frac{1}{5}$. Computations for other values of this ratio indicate that a given Landau level C splits up into two clusters of sub-bands. A number p of sub-bands goes upwards across the diagram as Q is increased, and $(\lambda-p)$ go downwards. The lowest level C in Fig. 8 is apparently an exception. Owing to the coincidence of two levels at LL the two clusters are kept together.

This splitting of each band into two clusters which are separated by a fairly substantial gap is obviously of interest when one calculates the effect of the band structure on the de Haas–van Alphen periods. It may lead to a modulation with a period of unity in F^{-1}, which corresponds to a Fermi-surface cross section equal to the area of the Brillouin zone in the two-dimensional model (Fig. 1).

A "topological" reason for this splitting of the bands into two clusters is easy to give. As F^{-1} is increased steadily, the levels C on the left of Fig. 6 move relative to the levels S and LL on the right by an amount given by (33). If all the states in a level C on the left were to recondense again into a unique level on the right, the increase in F^{-1} would cause a progressive shear of the structure, and the structure would not be periodic in F^{-1}. The splitting of the states in a level C into two clusters in the way described above eliminates this shear.

A physical reason for the appearance of a gap in each band may be given as follows, along the lines of an argument in a previous paper by the author.[4] Suppose the parameter Q_2 was set equal to zero, but Q_1 was left at some intermediate value, say 0.5. Then the lines of the orbits in Fig. 2 are decoupled in the y direction, but the electron can move at a fairly large speed along the orbits coupled along the x direction. Figure 11 shows a schematic plot of the energies E_l, E_{l-1} as a function of q_x for the lth and $(l-1)$th lines of orbits, respectively. The energy is periodic with a period of bh or $2\pi\lambda/Na$ in q_x, but the curves are displaced by a value of q_x equal to $bh(p/\lambda)$. This value is simply $g=2\pi/a$ modulo bh, and the displacement arises because of the structure of the equations (8) (with V_1 set equal to zero). Now suppose that Q_2 is switched on very slightly. Two energy gaps of the first order in Q_2 will form at A and B (Fig. 11) by hybridization. Other gaps will form corresponding to interactions between lines of orbits that are not neighbors, but these will be of higher order in Q_2. These first-order gaps however will not be of the same size for the following reason. A positive value of $\partial E/\partial q_x$ means a positive value of the velocity along Ox. This implies that the electronic wave function has a larger amplitude along the top of a line of orbits than along the bottom since the electron is effectively spending most of its time on an open orbit carrying electrons to the right. The converse applies for negative slopes. Thus, at A in Fig. 11 the slope of E_l is positive, so that the wave function is concentrated at the top of the lth line of orbits, and the slope of E_{l-1} is negative, so that the wave function is concentrated at the bottom of the $(l-1)$th line of orbits. For the point B the wave function is concentrated at the bottom of the lth line of orbits and at the top of the $(l-1)$th line of orbits. Figure 2 shows that the $(l-1)$th line of orbits is higher than the lth, and so the gap at A produced by hydridization would be expected to be larger than the gap at B. It would be reasonable to expect that the larger gap is the one responsible for the separation of the clusters.

A numerical computation verified this result. The same situation was chosen as in Fig. 8 with $p/\lambda=\frac{1}{5}$. But Q_1 was increased first to 0.5, with Q_2 remaining zero, and then Q_2 was increased to 0.5, with Q_1 remaining at 0.5. Figure 12 shows how a Landau level evolves into the situation at $Q=0.5$ shown in Fig. 8. As Q_1 is increased the Landau level broadens out into a band[1] as shown in Fig. 11. But as Q_2 is switched on, gaps appear. The gaps A and B are of first order in Q_2, but the gap A is rather wider than the gap B, and indeed it is the one which separates one sub-band from the other four.

We have discussed the possibility of having open hyperorbits. The question arises: Could they lead to a resonant ultrasonic attenuation analogous to the ultrasonic attenuation by ordinary open orbits? The hori-

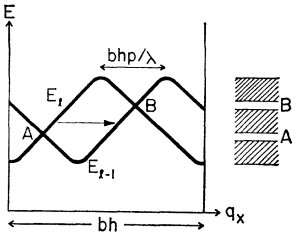

FIG. 11. Schematic plots of energy versus q_x for the lth and $(l-1)$th lines of orbits. Right-hand portion shows where gaps are formed in an energy band by hybridization.

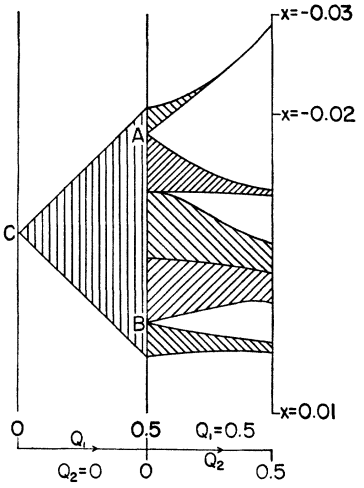

FIG. 12. Evolution of a Landau level when F^{-1} equals an integer plus $\frac{1}{5}$. On the left Q_2 is left equal to zero while Q_1 increases from 0 to 0.5, and on the right Q_1 is left equal to 0.5 while Q_2 increases from 0 to 0.5. The energy parameter increases downwards. The bands are shaded. Note that the gap A splits off one subband from the other four.

zontal arrow in Fig. 11 represents an electronic transition caused by a phonon absorption of a type previously suggested by the author.[4] It is easy to verify that the wave number of the absorbed phonon corresponds to the length of a period of an open hyperorbit as calculated from the "semiclassical" theory suggested above. Thus it may well be that the absorption can be described as an absorption by open hyperorbits. But open hyperorbits are not possible in a square or a hexagonal lattice because an open orbit requires that the magnetic field be aligned along an axis with twofold or onefold rotational symmetry. This does not rule out the possibility of having ultrasonic attenuation by a spatial resonance, since closed hyperorbits coupled by breakdown might also give the resonance. For the time being this must be regarded as a speculation.

5. CONCLUDING REMARKS

A method has been developed to extend Pippard's calculations of magnetic band structures in two-dimensional models to cases when the parameter F^{-1} is not just an even integer. The numerical results suggest two things. The first suggestion is that the band structure can be interpreted to some extent in terms of the concept of "hyperorbits." Such hyperorbits may even give rise to ultrasonic attenuation by a spatial resonance. The second suggestion is that when a Landau level for a free electron is broadened by the lattice potential it breaks into two clusters of sub-bands, and such a structure may give rise to unusual periodicities in the de Haas–van Alphen effect.

The investigation of the de Haas–van Alphen periodicities in the model has not yet been carried out and might lead to some interesting results. The fact that the band structure is a very sensitive function of the magnetic field leads to some difficulties here. The theory of magnetoresistance in the model would probably be much harder though the concept of hyperorbits might well be relevant, since they would share some of the properties of ordinary orbits.

ACKNOWLEDGMENTS

The author would like to thank the staff of the Physics Department at Texas A&M University and the staff of the Physics Department at the University of Texas for their kind hospitality. He also wishes to thank Professor E. Brown and Professor L. Falicov for helpful discussions.

APPENDIX

The problem of finding the dependence of the trace in (29) on α can be solved as follows. First we show that the trace is periodic in α with a period of $2\pi/\lambda$, not just of 2π. Since λ and N have no common factors it can be shown from (13) that

$$\alpha_l+2\pi/\lambda=\alpha_{l+p} \text{ modulo } 2\pi$$

for a fixed integer p. Thus increasing α by $2\pi/\lambda$ cyclically permutes the matrices $\mathbf{K}_l$ in (28), and therefore the trace in (29) is unaltered.

Since the highest power of $e^{\pm i\alpha}$ that can appear is λ, the trace must have the form

$$\mathrm{Tr}\{(\mathbf{T}(\alpha)\}=\kappa e^{i\lambda\alpha}+\mu+\nu e^{-i\lambda\alpha}.$$

The coefficient κ can be obtained as follows. Let us divide each matrix $\mathbf{K}_l$ by $e^{i\alpha l}$. The product of these divisors is readily shown to be $-(-1)^\lambda e^{i\lambda\alpha}$. Then κ is the value of the new trace with $\alpha=-i\infty$, multiplied by $-(-1)^\lambda$. For $\alpha=-i\infty$ we have

$$e^{-i\alpha l}\mathbf{K}_l=\begin{pmatrix}0 & 0\\ B^* & 0\end{pmatrix}$$

by (19b), and so it follows that

$$e^{-i\alpha l}\mathbf{M}\mathbf{K}_l=\frac{B^*}{b^*}\begin{pmatrix}-1 & 0\\ -a^* & 0\end{pmatrix}$$

by (24b). This matrix is then raised to the power λ, and the trace is found to be $(-B^*/b^*)^\lambda$. Hence

$$\kappa=-(B^*/b^*)^\lambda$$

which is real by (23b) and (24d). Similarly it can be shown that

$$\nu=-(B/b)^\lambda.$$

The coefficient μ is obtained by evaluating $\mathrm{Tr}[\mathbf{T}(0)]$, and hence

$$\mathrm{Tr}[\mathbf{T}(\alpha)]=-2(B/b)^\lambda(\cos\lambda\alpha-1)+\mathrm{Tr}[\mathbf{T}(0)].$$

With this result, (30) can be derived very simply from (29).